

Initial Studies of the Bidirectional Reflectance Distribution Function of Carbon Nanotube Structures for Stray Light Control Applications

James J. Butler^a, Georgi T. Georgiev^b, June L. Tveekrem^c, Manuel Quijada^c, Stephanie Getty^d, John G. Hagopian^c

^aNASA Goddard Space Flight Center, Code 614.4 Biospheric Sciences Branch, Greenbelt, MD 20771

^bSigma Space Corporation, 4400 Lottsford Vista Road, Lanham, MD 20706

^cNASA Goddard Space Flight Center, Code 551.0 Optics Branch, Greenbelt, MD 20771

^dNASA Goddard Space Flight Center, Code 541 Materials Engineering Branch, Greenbelt, MD 20771

ABSTRACT

The Bidirectional Reflectance Distribution Function (BRDF) at visible and near-infrared wavelengths of Multi-Wall Carbon NanoTubes (MWCNTs) grown on substrate materials are reported. The BRDF measurements were performed in the Diffuser Calibration Laboratory (DCaL) at NASA's Goddard Space Flight Center, and results at 500nm and 900nm are reported here. In addition, the 8° Directional/Hemispherical Reflectance of the samples is reported from the ultraviolet to shortwave infrared. The 8° Directional/Hemispherical Reflectance was measured in the Optics Branch at NASA's Goddard Space Flight Center. The BRDF was measured at 0° and 45° incident angles and from -80° to +80° scatter angles using a monochromatic source. The optical scatter properties of the samples as represented by their BRDF were found to be strongly influenced by the choice of substrate. As a reference, the optical scattering properties of the carbon nanotubes are compared to the BRDF of Aeroglaze Z306™ and Rippey Ultrapol IV™, a well-known black paint and black appliqué, respectively. The possibility, promise, and challenges of employing carefully engineered carbon nanotubes in straylight control applications particularly for spaceflight instrumentation is also discussed.

Keywords: multiwalled carbon nanotubes, bidirectional reflectance distribution function, 8° directional/hemispherical reflectance, silicon

1. INTRODUCTION

Satellite-based earth and space observations present scientists and engineers with two extreme challenges in remote sensing. From low orbit, the Earth appears as a bright target of large angular extent. Quantitative remote sensing of that part of the Earth within the field of view of a satellite instrument is comprised of light both within and outside the instrument field of view. This is often termed the size of source effect. Light which enters the instrument is then diffracted and scattered by internal instrument structures, adversely impacting remote sensing measurements. In contrast, space-based astrophysical observations often require the detection and measurement of light originating from small, distant, often faint objects. These observations are also highly susceptible to scattered light which serves to obscure the remotely sensed object and contributes to increase measurement noise. Scattered light is often

controlled by the use of light tight enclosures equipped with strategically placed baffles and stops. In addition to placement, a low bidirectional reflectance of these structures is key in the reduction of scattered light within an instrument.

The scientific benefits of reducing stray or scattered light within a remote sensing instrument can be illustrated for the case of ocean color/chlorophyll (OCC) retrievals. Satellite remote sensing of OCC is probably the most radiometrically challenging and climate sensitive Earth science measurement. The radiometric challenge lies in that OCC is derived from measurements of water leaving radiance which is approximately $1/10^{\text{th}}$ the total signal detected by the satellite instrument due to atmospheric scattering effects. In addition, the ocean is an optically dark target dotted with numerous bright clouds. Measurements of OCC, therefore, are adversely affected by instrument near and far field stray light originating from optical scatter from reflective and transmissive optics, baffles, vanes, cavities, and stops. Figure 1 shows two images of chlorophyll concentration derived from the SeaWiFS satellite instrument off the coast of Chile. In both images, the yellow, green, and blue colors represent pixels where chlorophyll was confidently retrieved. In the left image, the black pixels represent areas where chlorophyll was not able to be retrieved, as in regions covered by clouds. The red pixels in the image on the right shows the extent of the regions in the left image which were contaminated by instrument stray light. Reduction of instrument stray light would enable chlorophyll to be confidently retrieved in all red areas, leading to 32% more scientifically useful pixels.

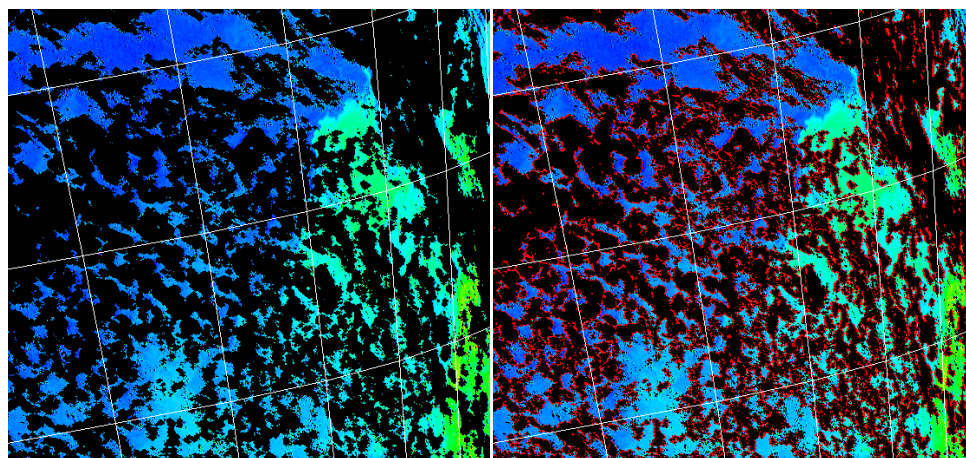


Figure 1. Images of chlorophyll concentration derived from SeaWiFS off the coast of Chile. The green, yellow, and blue pixels represent areas where chlorophyll was successfully retrieved. The black pixels represent areas where chlorophyll could not be retrieved, such as in cloudy regions. The red pixels in the right image indicate those pixels from the left image which were contaminated by stray light. Elimination of stray light for those pixels in red would result in an increase of 32% in scientifically useful pixels.

The ideal surface for the reduction of instrument stray light should have a uniform low reflectance independent of light incident angle and the wavelength. Internal instrument scattered light is typically reduced using a number of black surface treatments. These treatments include paints, appliques, and etched, electro-deposited and sprayed metal surfaces. A number of excellent publications, reviews, and databases on the optical properties of black surfaces and materials have been published and compiled [1-21]. The choice of treatment depends strongly on the geometry, application, operating wavelength range, and, for the specialized case of space instrumentation, optical and mechanical stability in the on-orbit environment.

2.1.1 Growth on Silicon Substrates

Vertically oriented MWCNT films were realized using catalyst-assisted chemical vapor deposition (CVD). Using silicon as the growth substrate, the fabrication began with the thermal deposition of aluminum/iron thin film catalyst. To grow MWCNTs, the substrate was exposed to ethylene feedstock gas at 750°C in a reducing environment; the ethylene was dissociated at the iron surface; and the carbon was extruded in the form of a dense film of aligned MWCNTs. Precise patterning of the MWCNT film was accomplished by constraining the placement of the catalyst film through conventional lithographic means. Varying the catalyst thickness on the substrate was used to modulate the MWCNT height.

2.1.2 Enhanced Adhesion on Silicon

Carbon nanotubes grown on silicon with only the iron catalyst layer were found to exhibit poor adhesion, and it was quite easy to rub the nanotubes off of the substrate. Utilization of MWCNTs in space flight hardware requires that they are robust to prevent degradation of the coating or contamination of critical components. Since previous work suggests that the point of failure is at the catalyst-substrate interface, alternative substrate preparation techniques were explored to improve adhesion. The primary approach involved the use of a thin film sticking layer under the iron catalyst layer. Experiments were conducted using chromium, titanium and alumina underlayers. The approach was straightforward and should not have significantly impacted the favorable properties of the thin Fe catalyst film. However, it was discovered that the nanotube growth properties were significantly affected by this layer. After much trial and error, it was determined that alumina provided the best sticking layer.

2.1.3 Growth on Alternate Materials

While it is quite feasible to use silicon for a variety of elements in space flight instrumentation including mirrors, slits and small blocking elements such as coronagraphic masks, silicon is quite brittle and is not the material of choice for elements that may be subjected to structural loads such as baffles and stops. To address the need for nanotube growth on materials that were more suitable for these elements we grew nanotubes on alternate materials at GSFC. The substrates investigated at GSFC included stainless steel, nickel, and titanium using the same thickness of iron catalyst layer and growth parameters optimized on the silicon substrates.

2.2 OPTICAL MEASUREMENTS

The darkness of prepared MWCNT samples was evaluated through measurements of their 8° directional/hemispherical reflectance from 300nm to 2000nm and bidirectional reflectance distribution function (BRDF) at 500nm and 900nm. The 8° directional/hemispherical reflectance measurements were performed first and were used to initially screen samples as candidates for follow-on BRDF measurements. These measurement approaches are described below.

2.2.1 8° Directional/Hemispherical Reflectance

8° directional/hemispherical reflectance is a measure of all light that is scattered off of a test sample. The instrument used to measure the 8° directional/hemispherical reflectance is a double monochromator-based Perkin Elmer Lambda 950 instrument equipped with an integrating sphere accessory as shown in figure 3. The reference and sample paths of this double beam instrument are shown in this figure. Light enters the integrating sphere through either the reference or sample port. The reference beam enters the integrating sphere via a rectangular port adjacent to M5. The sample beam is reflected into the sphere directly off mirror M2 and onto the sample to be measured. By illuminating the sample under test at 8° from its normal, the specularly reflected beam is detected in addition to all non-specular scatter. This configuration allows the capture of all the reflected light from the sample. This light detection is done

by two detectors located inside the sphere: a R955 photomultiplier tube (PMT) for the wavelength range from 300 and 860 nm a lead sulfide (PbS) detector to cover the 860-2000 nm region. Finally, the inside of the sphere is coated with a Spectralon™. Because the measurement of directional/ hemispherical reflectance does not discriminate the angle of reflectance but measures the total amount of reflected light, directional/hemispherical reflectance is a good measure of the relative ability of a sample to absorb light. In this study, it is used as a screening tool to determine if a particular sample is effective at absorbing light and warrants further BRDF characterization.

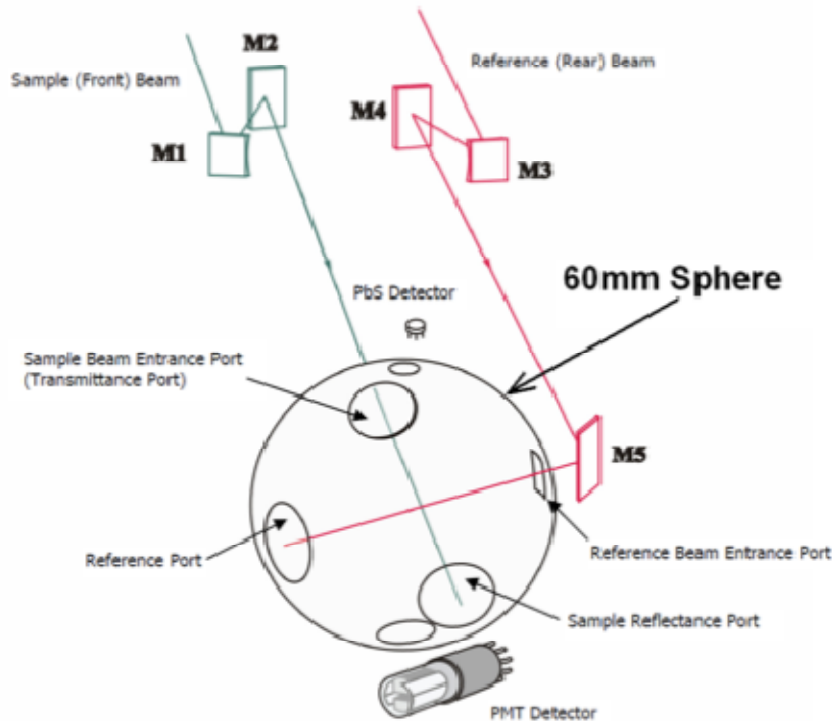


Figure 3. The 8° directional/hemispherical reflectance measurement accessory in the PE Lambda 930 instrument.

2.2.2 Bidirectional Reflectance Distribution Function (BRDF)

While directional/hemispherical reflectance quantifies the total amount of light that is reflected over all angles, it does not provide sufficient directional information required to model stray light reaching the focal plane of an optical system. Light passing through an instrument optical system can be blocked by instrument components such as baffles and stops, reflected and scattered by mirrors, and transmitted and scattered by refractive optics, windows, tubes, and filters. NASA utilizes detailed ray-tracing models that deterministically calculate the trajectory of all light that propagates through an optical system. For mirrors and optical elements, measurements of the surface figure and micro-roughness and allocations for contamination are required as input to these models. For structural elements and stray light controls such as baffles, tubes and stops, the distribution of light as a function of incident and scatter angles is required. The bidirectional reflectance distribution function (BRDF) fully defines the directional reflection characteristics of a surface. It provides the reflectance of a target in a specific direction as a function of illumination and viewing geometry. The BRDF is a function of wavelength and reflects the structural and optical properties of the surface. The BRDF definition and derivation are credited to Nicodemus et al. [29] who examined the problem of defining and measuring the scatter of diffuse and specular optical materials. Following his

concept the scatter defining geometry is shown in Figure 4, where the subscripts i and s refer to incident and scatter quantities, respectively.

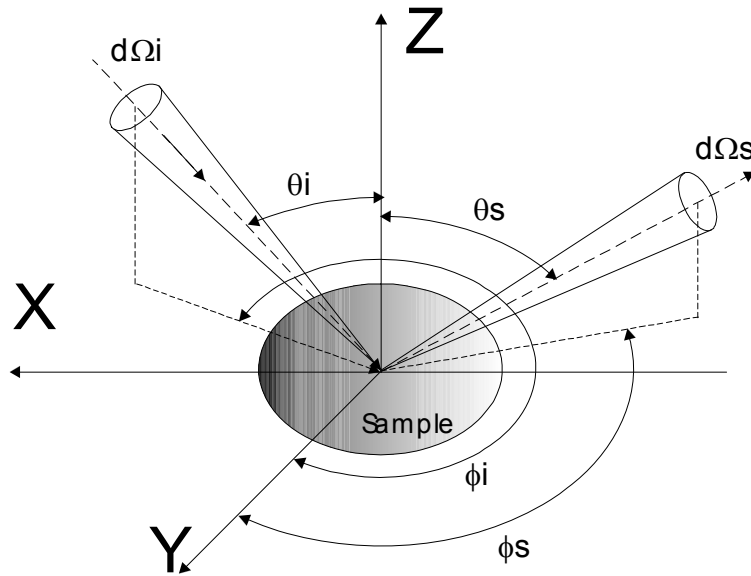


Figure 4. BRDF scattering geometry

Nicodemus also assumed that all scatter comes from the sample surface and none from the bulk. He defined the BRDF in radiometric terms as the ratio of the surface radiance, L_s , scattered by a surface into the direction (θ_s, ϕ_s) to the incident surface irradiance, E_i , incident on a unit area of the surface at a particular wavelength, λ , as shown in Equation 1.

$$BRDF = \frac{L_s(\theta_i, \phi_i, \theta_s, \phi_s, \lambda)}{E_i(\theta_i, \phi_i, \lambda)} = \frac{P_s / \Omega}{P_i \cos \theta_s} \quad (1)$$

In equation 1, the subscripts i and s denote incident and scattered respectively, θ the zenith or elevation angle, and ϕ the azimuth angle.

The various carbon nanotube samples were measured in the Diffuser Calibration Laboratory (DCaL) at NASA's Goddard Space Flight Center (GSFC) using the facility's scatterometer. The scatterometer, located in a class 10000 laminar flow cleanroom, is capable of measuring the bidirectional scatter distribution function (BSDF) of a wide range of sample types including white diffusers, gray-scale diffusers, black painted or anodized diffusers, polished or roughened metal surfaces, clean or contaminated mirrors, transmissive diffusers, liquids, and granular solids. BSDF includes BRDF and the bidirectional transmissive distribution function (BTDF). The instrument is an out-of-plane scatterometer capable of measuring optical scatter above or below any sample. The operational spectral range of the instrument is continuous from 230 nm to 900 nm and at select laser wavelengths in the shortwave infrared. The scatterometer data acquisition and display is completely computer controlled. The measurement uncertainty, $\Delta BRDF$, depends on several instrument variables. It was evaluated in the ultraviolet through near infrared in accordance with NIST guidelines [30] to be less than 0.7% ($k=1$). The main sources of uncertainty are 1) signal to noise ratio; 2) nonlinearity of the detector and electronics; 3) receiver solid angle; and 4) the total scatter angle error.

The main sources of error are considered independent. Schiff et al. [31] presents the detailed study of this measurement uncertainty. Figure 5a is a side-view diagram of the goniometer stages of the scatterometer. Figure 5b is a photograph of the monochromator source, chopper, polarizer and circular and fold mirrors. The last two mirrors send the monochromatic beam through a hole in the optical table to the sample side of the scatterometer. Figure 5c is a photograph of the sample side of the scatterometer featuring the sample and detector stages. The scattered light from the sample is collected using an ultraviolet-enhanced silicon photodiode detector with output fed to a computer-controlled lock-in amplifier. The sample is mounted on a stage in the horizontal plane. The sample stage allows precise positioning of the sample with respect to the incident beam and can be moved in X, Y, and Z linear directions using three motors. The sample stage provides sample rotation in the horizontal plane around the Z axis enabling changes in the incident azimuth angle, ϕ_i . Sample stage leveling is adjusted using two manual micrometers. Sample holders are custom designed to support samples of different sizes, shapes, and thicknesses.

3. RESULTS AND DISCUSSION

8° directional/hemispherical and BRDF measurements on the following three GSFC samples are presented in this paper: MWCNTs on silicon, enhanced adhesion MWCNTs on silicon using an alumina underlayer, and MWCNTs on titanium. Comparisons are also made to the reflectance properties of Z306, a black paint commonly used on spaceflight surfaces, and Ultrapol IV, a black appliqué used in laboratory instrument stray light reduction. Figures 6 to 8 are scanning electron microscope (SEM) images of the three MWCNT samples. Figure 6 shows vertically oriented MWCNTs on silicon.

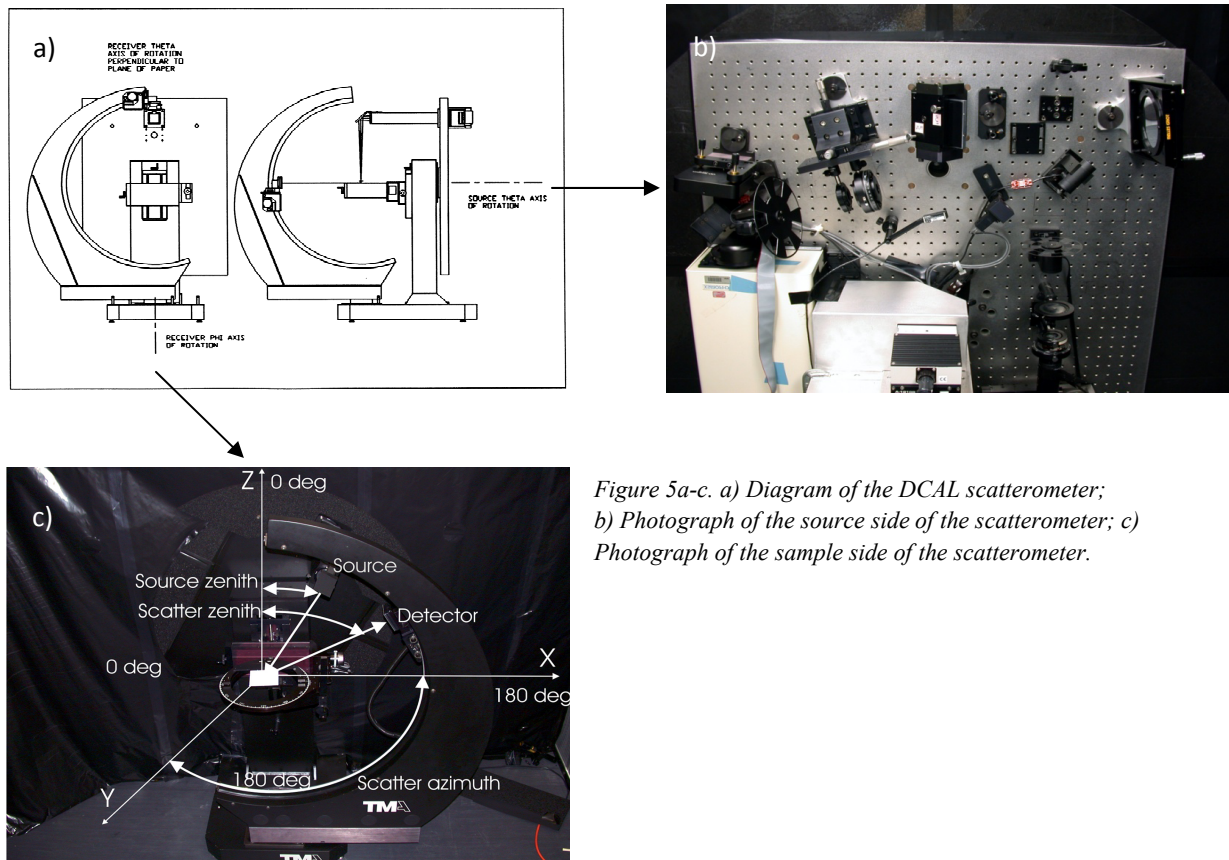


Figure 5a-c. a) Diagram of the DCAL scatterometer; b) Photograph of the source side of the scatterometer; c) Photograph of the sample side of the scatterometer.

Figure 7 is an SEM image of a section of nanotubes deposited on silicon using an alumina underlayer to enhance adhesion. The nanotubes in this figure have been removed from the substrate for purposes of inspection. The film appears uniform, vertically oriented, and was more robust to physical contact than the sample deposited on pure silicon. Figure 8 is an SEM image of MWCNTs deposited on a titanium substrate. The nanotube growth on this sample appears wire-like with random arrangements of curled nanotubes.

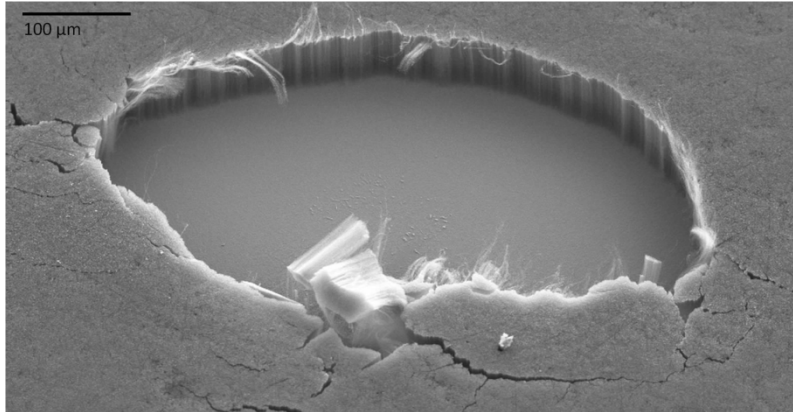


Figure 6. MWCNTs on silicon substrate.

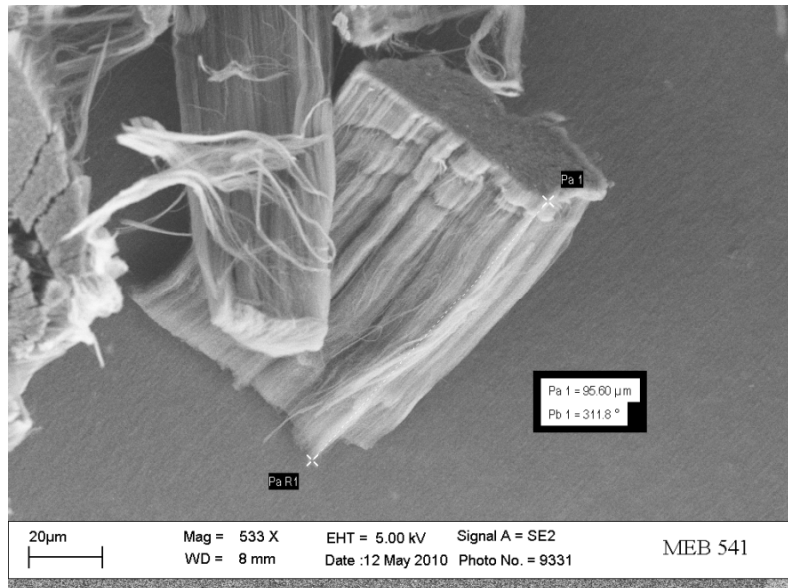


Figure 7. MWCNTs on silicon substrate with alumina underlayer for enhanced adhesion.

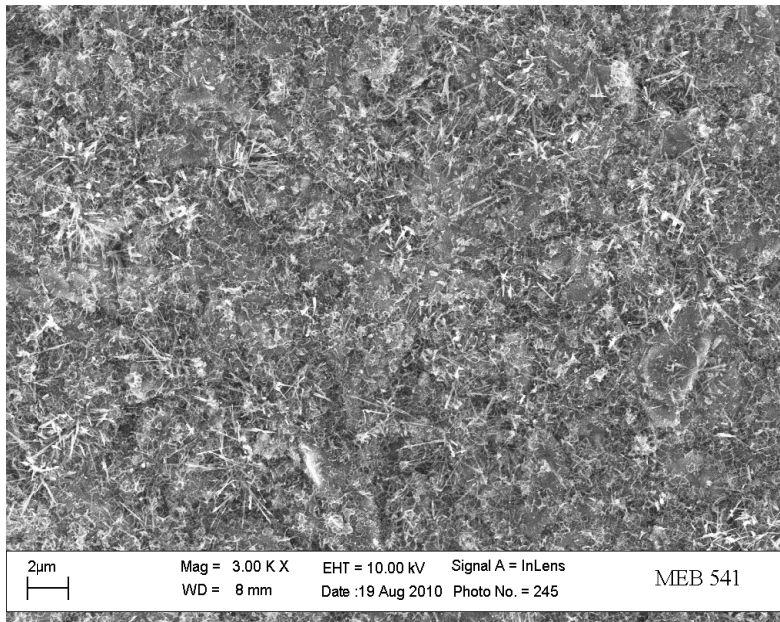


Figure 8. MWCNTs on titanium substrate.

8° directional/hemispherical reflectance measurements on the three MWCNT samples and Z306 paint are shown in figure 9.

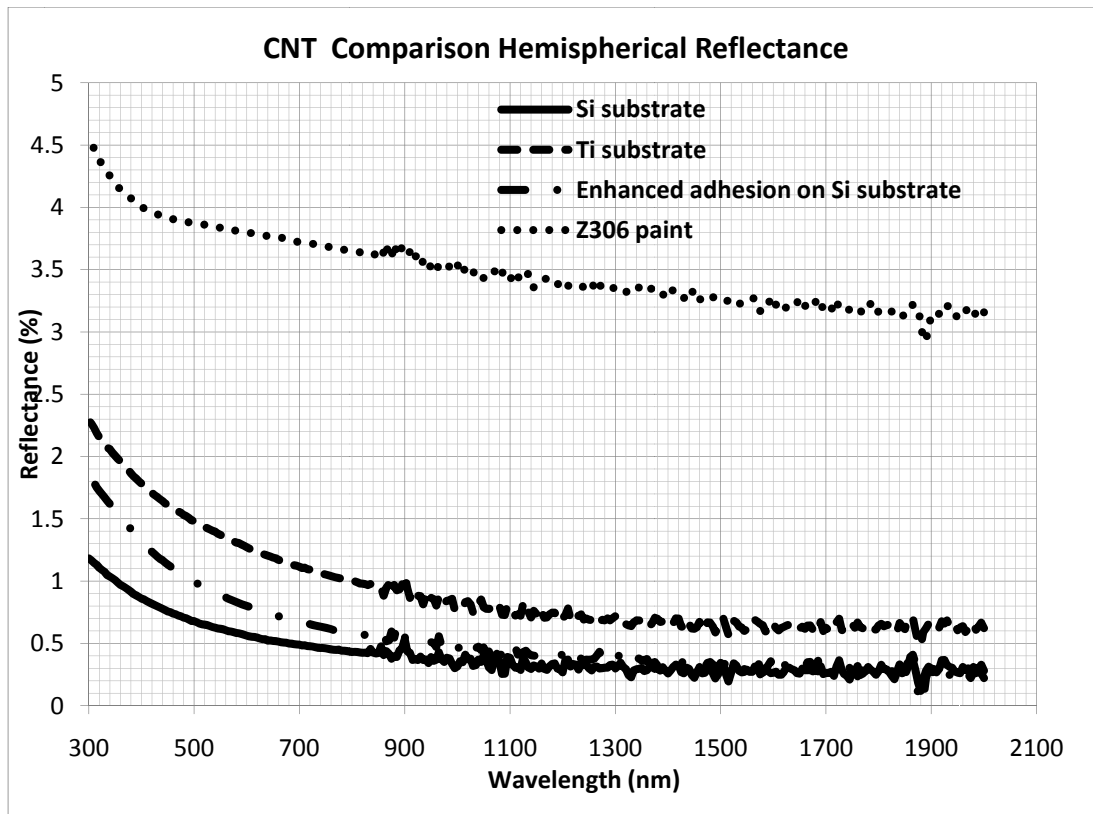


Figure 9. 8° directional/hemispherical reflectance of the three MWCNT samples and Z306 paint.

In figure 9, the directional/hemispherical reflectance of the MWCNT sample on the silicon substrate produced the lowest reflectance values. These values were 4.5 to 10 times lower than the directional/hemispherical reflectance of Z306 paint over the wavelength range shown. The nanotube sample with the highest reflectance was the MWCNT sample on the titanium substrate. It should be noted that this sample was still 2 to 5 times darker than the Z306 sample over the ultraviolet to shortwave infrared wavelength range. The enhanced adhesion MWCNT sample on the silicon substrate produced reflectance values which were 1.8 to 10 times lower than Z306.

The BRDF of these samples, Z306 paint, and the black appliqué, Ultrapol IV™, are shown in figures 10 and 11 at 500 nm and 900 nm, respectively, at normal illumination.

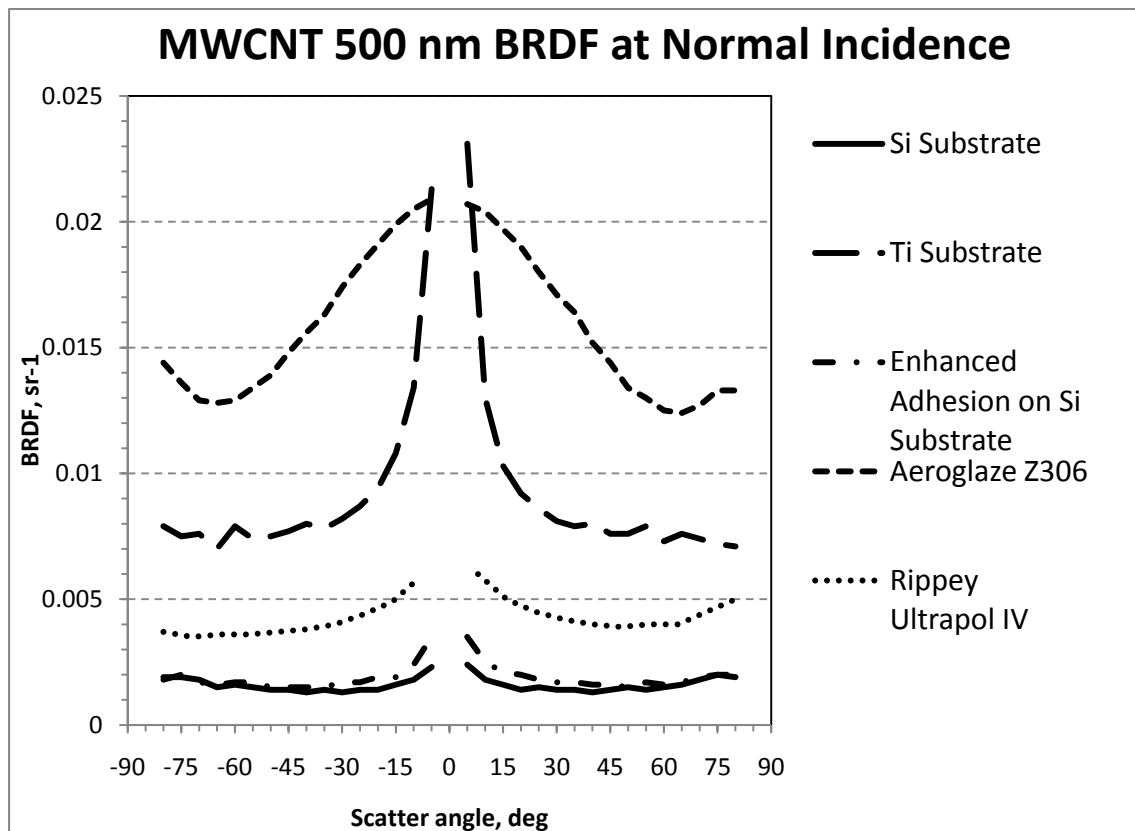


Figure 10. 500 nm BRDF of MWCNT samples, Z306, and Ultrapol IV™ at normal incidence.

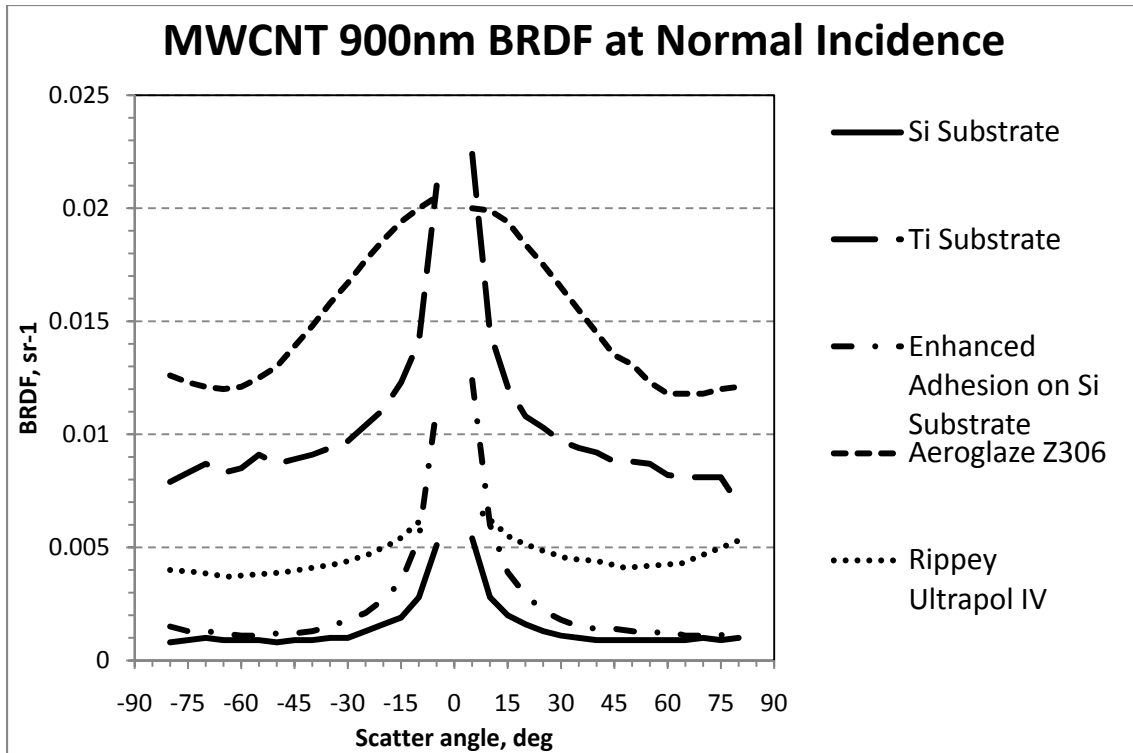


Figure 11. 900 nm BRDF of MWCNT samples, Z306, and Ultrapol IV™ at normal incidence.

Since integration of the 8° directional/hemispherical reflectance over the complete scattering hemisphere of a sample produces that sample's BRDF, the normal incident BRDF data shown in figures 10 and 11 follow the directional hemispherical reflectance data. That is, the directional/hemispherical and BRDF data predict the Si substrate C nanotube sample to be the darkest, followed by the enhanced adhesion sample and the Ti substrate C nanotube sample. Interesting effects are seen in the BRDF data in the vicinity of 0° scatter, i.e. the direction of retroreflection. Deviation from constant BRDF in these curves is an indication of the degree of non-Lambertian reflectance behavior. The Ti substrate C nanotube sample shows the largest and sharpest retroreflectance, followed by the enhanced adhesion sample and the Si substrate C nanotube sample. Sources of retroreflection in these samples include reflection off the tube edges and reflection off the base substrate material of the tubes. Z306 paint exhibits the highest BRDF at both 500 and 900 nm, while Ultrapol IV exhibits the most Lambertian behavior.

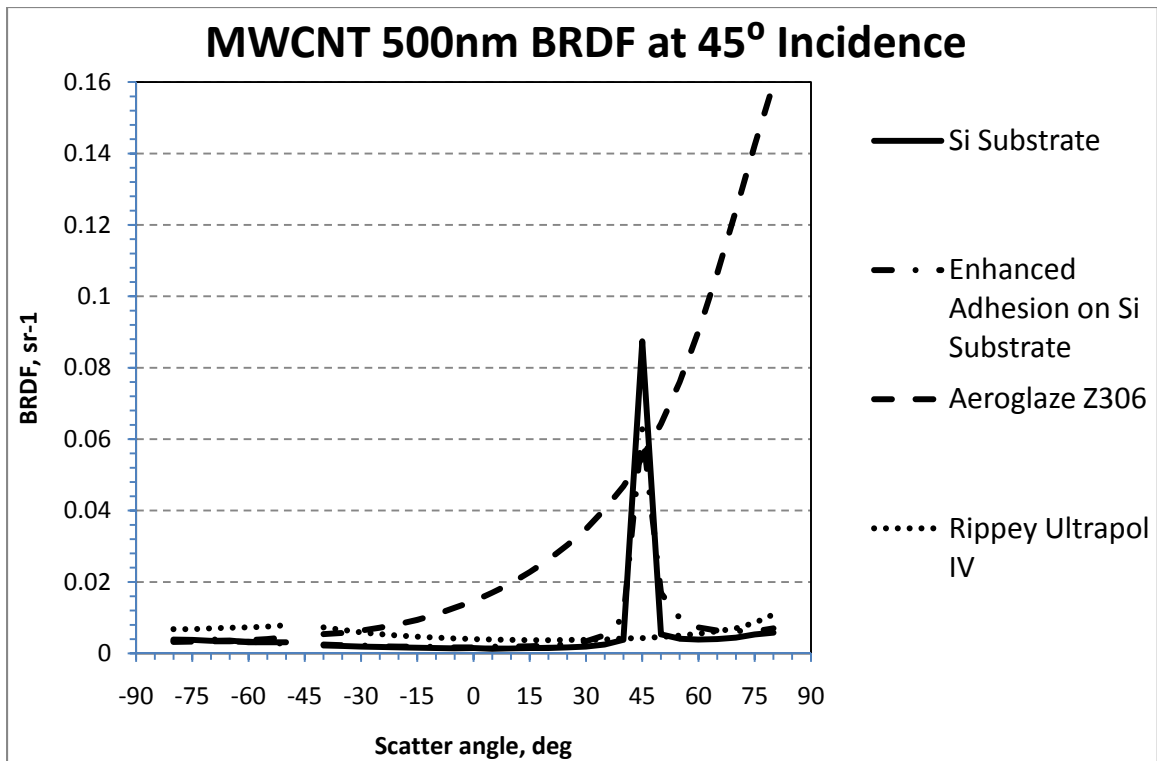


Figure 12. 500 nm BRDF of Si substrate and Enhanced Adhesion MWCNT samples, Z306, and Ultrapol IV™ at 45° incidence.

The BRDF of the Si substrate C nanotube sample, the enhanced adhesion nanotube sample, Z306 paint, and the black appliqué, Ultrapol IV™, are shown in figures 12 and 13 at 500 nm and 900 nm, respectively, at 45° illumination. Both the Si substrate and enhanced adhesion MWCNT samples exhibit the lowest reflectance at angles away from specular. However, at the specular angle, both nanotube samples show appreciable BRDF peaks. This specular reflectance is possibly originating from the tops of the nanotubes. Interestingly, there is no evidence of retroscatter in the MWCNT samples. Retroscatter, if present, would originate from reflectance off the illuminated insides of the nanotubes. The lack of retroscatter indicates that light illuminating the insides of the nanotubes is undergoing multiple reflections down the length of the tubes. The strong forward scatter of the Z306 paint is characteristic of a one-bounce surface scattering process. Once again, the Ultrapol IV™ appliqué exhibits virtually no forward scatter and small retroscatter, characteristic of a near Lambertian scattering surface.

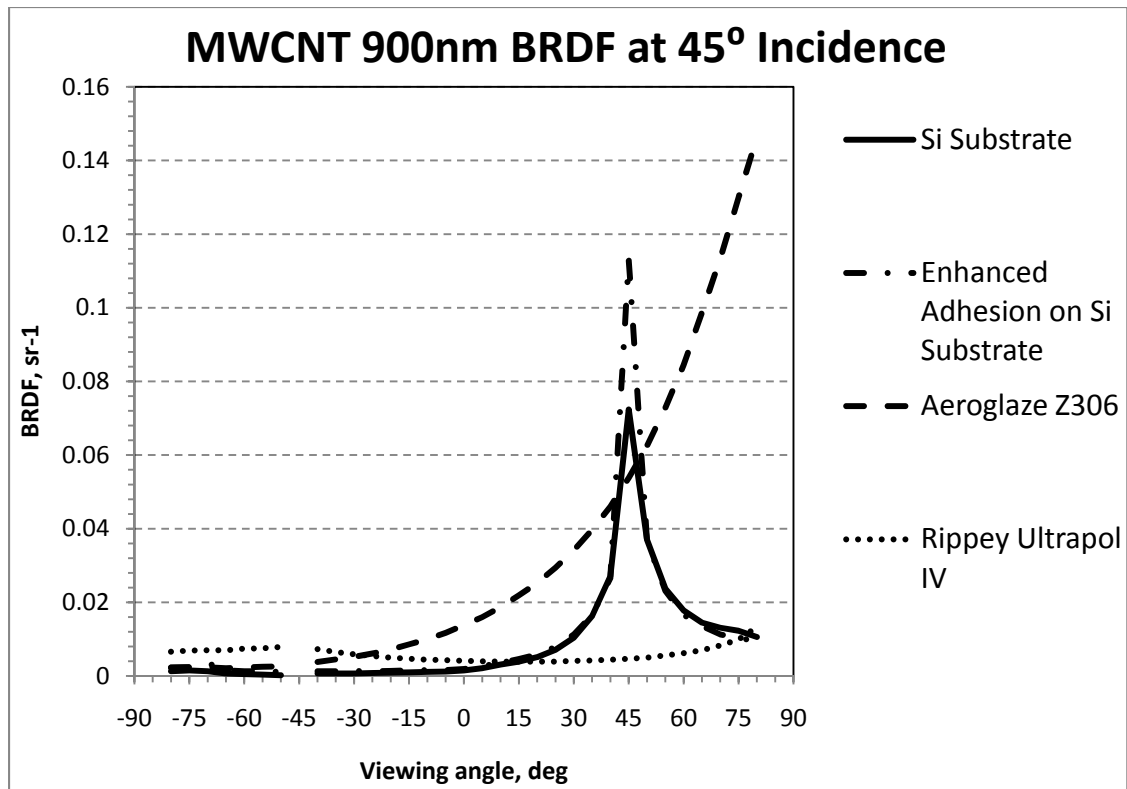


Figure 13. 900 nm BRDF of Si substrate and Enhanced Adhesion MWCNT samples, Z306, and Ultrapol IV™ at 45° incidence.

The goal of this research was to utilize MWCNTs in an effort to achieve an order of magnitude lowering of visible reflectance exhibited by black paints and surface treatments currently employed in spacecraft instrument stray light control. From the 8° directional/hemispherical reflectance data, the factor of 10 reduction in reflectance over Z306 paint was realized only for the MWCNTs on silicon substrates and at wavelengths above 1100 nm. For the silicon substrate samples below 1100nm and for the titanium substrate sample, the reduction in reflectance was from 2 to 10 times. In order to realize an order of magnitude reduction in reflectance in the ultraviolet through near infrared, several approaches for optimization of MWCNT geometry are being examined. One approach being examined is to employ oxygen plasma etching to add roughness and porosity to MWCNT films. The effect of this plasma etching process is shown in the SEM images in figure 14. In addition to plasma etching, surface roughness is being exploited to engineer the morphology of catalyst-assisted thermal chemical vapor deposition grown MWCNT films. The effects of modulating the catalyst film thickness to produce low density, tall nanotubes are also being examined [32]. The process used in this study resulted in multi-walled carbon nanotubes with typical inner diameters of 1 to 5 nm, outer diameters of 30 to 100 nm and an average spacing of 100 to 500 nm. The best samples had lengths of 50 to 100 microns, but it is highly probable that longer lengths would provide better performance. This area is being actively pursued since researchers at Rensselaer Polytechnic Institute have reported achieving even higher absorption with longer nanotubes [22].

The BRDF data on the MWCNT samples provided important detailed insight into their geometric reflectance properties. The absence of significant retro- and the presence of forward-reflected specular

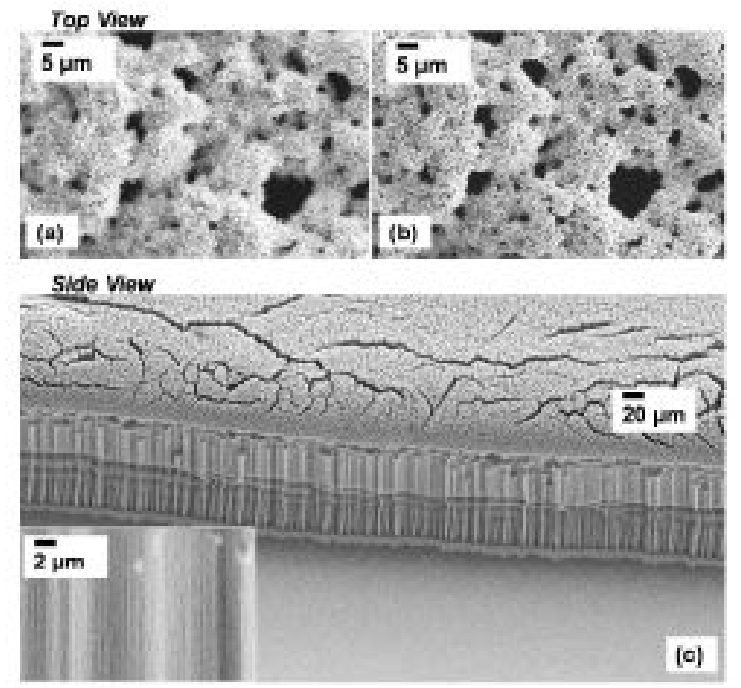


Figure 14a-c. a) Top view of MWCNTs on silicon substrate. b) MWCNTs following treatment with oxidizing plasma, producing a larger pore size. c) Low magnification view of the sample shows well-aligned MWCNTs.

features in the BRDF of the nanotube samples must be accounted for in any instrument stray or scattered light control application. In parallel with work in reducing the overall reflectance from MWCNT samples, research on the reduction of sample specular reflectance is underway in addition to the acquisition of more extensive BRDF measurements at additional wavelengths, incident, and scatter angles.

4. CONCLUSIONS

Initial studies of MWCNT structures deposited on the substrates presented in this paper show potential for lowering stray and scattered light in optical instrumentation. Normally illuminated MWCNTs on a silicon substrate were found to be 4 to 10 times darker at 500 nm and 900 nm than Z306, a commonly used black paint used in spacecraft instrument applications. Enhanced adhesion nanotubes and nanotubes on a titanium substrate resulted in reflectances which were higher than the initial silicon substrate sample but still darker than spacecraft black paint. Illumination at 45° interestingly produced specular peaks in the nanotube samples' BRDFs. It is hoped that additional engineering techniques in the production of nanotubes, such as plasma etching and control of tube growth length, will be able to suppress specular features while further lowering overall sample reflectance. The work presented in this paper constitutes only the initial steps in examining the potential of using MWCNTs in spacecraft instrument stray light suppression applications. A significant amount of engineering and testing is required to ultimately qualify MWCNTs for space use. Some of this testing is currently underway at NASA. NASA is acquiring optical measurements at additional wavelengths from the ultraviolet through shortwave infrared on MWCNT samples deposited on a variety of substrates. In addition, NASA is performing more complete characterization of sample optical scatter over a wide range of in- and out-of plane incident and scatter angles. In parallel with optical testing, NASA continues to explore alternate deposition techniques on common spacecraft materials with the goal of increasing the MWCNT sample mechanical strength and stability.

5. REFERENCES

1. Pompea, S.M. and R.P. Breault, "Characterization and Use of Black Surfaces for Optical Systems," Chapter 6 in the *Handbook of Optics, Vol. IV*, Optical Properties of Materials, M. Bass, ed., McGraw Hill, pp. 6.1-6.67, 2010.
2. McCall, S.H.C.P., S.M. Pompea, R.P. Breault, and N.L. Regens, "Reviews of Black Surfaces for Space and Ground-based Optical Systems," Proc. SPIE, 1753, 158-170, 1992.
3. Kodama, S., M. Horiuchi, T. Kunii, and K. Kuroda, "Ultra-black Nickel-Phosphorus Alloy Optical Absorber," IEEE Transactions on Instrumentation and Measurement, 39, 230-232, 1990.
4. Persky, M.J., "Review of Black Surfaces for Space-borne Infrared Systems," Rev. Sci. Instrum. 70, 2193-2217, 1999.
5. Viehmann, W. and R. E. Predmore, "Ultraviolet and Visible BRDF Data on Spacecraft Thermal Control and Optical Baffle Materials," Proc. SPIE, 675, 67-72, 1986.
6. Pompea, S.M., D.F. Shepard, and S. Anderson, "BRDF Measurements at 6328 Angstroms and 10.6 Micrometers of Optical Black Surfaces for Space Telescopes," Proc. SPIE, 967, 236-247, 1988.
7. McCall, S.H.C.P., "Black Materials Database of Stellar Optics Laboratories, 78 Normark Drive, Thornhill, Ontario, Canada, L3T 3R1, 1992.
8. Ames, A.J., "Z306 Black Paint Measurements," Proc. SPIE, 1331, 299-304, 1990.
9. Betts, D.B., F.J.J. Clarke, I.J. Cox, and J.A. Larkin, "Infrared Reflection Properties of Five Types of Black Coating for Radiometric Detectors," J. Phys. E.: Sci. Instrum., 18, 689-696, 1985.
10. Brown, R.J.C., P.J. Brewer, and M.J.T. Milton, "The Physical and Chemical Properties of Electroless Nickel-Phosphorus and Low Reflectance Nickel-Phosphorus Black Surfaces," J. Mater. Chem., 12, 2749-2754, 2002.
11. Meier, S.R., M.L. Korwin, and C.I. Merzbacher, "Carbon Aerogel: A New Nonreflective Material for the Infrared," Appl. Opt. 39, 3940-3944, 2000.
12. Snail, K.A., D.P. Brown, J. Constantino, W.C. Shemano, C.W. Schmidt, W.F. Lynne, C.L. Seaman, and T.R. Knowles, "Optical Characterization of Black Appliques," Proc. SPIE, 2864, 465-474, 1996.
13. Jager, C., Th. Henning, R. Schlogl, and O. Spillecke, "Spectral Properties of Carbon Black," J. Non-Cryst. Solids, 258, 161-179, 1999.
14. McCall, S.H.C.P., L.B. Begrambekov, and J.E. Pierre, "A Review of Black and Reflective Spectrally Selective Surfaces Developed in the Former U.S.S. R.," Proc. SPIE, 2260, 178-181, 1994.
15. Miller, J.L., "Multispectral Infrared BRDF Forward-scatter Measurements of Common Black Surface Preparations and Materials-or "How Black is Black in the IR?," Proc. SPIE, 5405, 25-35, 2004.
16. Smith, S.M., "Specular Reflectance of Optical Black Coatings in the Far Infrared," Appl. Opt. 23, 2311-2326, 1984.
17. Smith, S.M., "Far Infrared Reflectance Spectra of Optical Black Coatings," Proc. SPIE, 362, 57-59, 1982.
18. Pompea, S.M., D.F. Berener, D.W. Shepard, S. Russak, and W.L. Wolfe, "Reflectance Measurements on an Improved Optical Black for Stray Light Rejection from 0.3 to 500 Micrometers," J. Opt. Eng., 23, 149-152, 1984.
19. Brown, C.W. and D.R. Smith, "High Resolution Spectral Reflectance Measurements on Selected Black Baffle Coatings in the 5-20 Micrometer Region," Proc. SPIE, 1331, 210-240, 1990.
20. Nee, S.M. and H.E. Bennett, "Characterization of Optical Blacks by Infrared Ellipsometry and Reflectometry," Proc. SPIE, 1331, 249-260, 1990.
21. Smith, S.M., "The Reflectance of Ames 24E, Infrablack, and Martin Black," Proc. SPIE 967, 248-254, 1988.
22. Yang, Z.P., L. Ci, J.A. Bur, S.Y. Lin, and P.M. Ajayan, "Experimental Observation of an Extremely Dark Material Made by a Low Density Nanotube Array," Nanoletters, 8, 446-451, 2008.
23. Wang, X.J., J.D. Flicker, B.J. Lee, W.J. Ready, and Z.M. Zhang, "Visible and Near-infrared Radiative Properties of Vertically Aligned Multi-walled Carbon Nanotubes," Nanotech., 20, 215704.1-215704.9, 2009.

24. Hagopian, J.G., S.A. Getty, M. Quijada, J. Tveekrem, R. Shiri, P. Roman, J. Butler, J. Livas, C. Hunt, A. Maldonado, S. Talapatra, X. Zhang, S. J. Papadakis, A. Monica, and D. Deglau, "Multiwalled Carbon Nanotubes for Stray Light Suppression in Space Flight Instruments," Proc. SPIE, 7761, 77610F-1-77610F-10, 2010.
25. Radushkevich, L.V. and V.M. Lukyanovich, "O Struktura Ugleroda, Obrazujucesgosja Pri Termiscekom Razlozenii Okisi Ugleroda Na Zeleznom Kontakte," Zurn. Fisic. Chim., 26, 88-95, 1952.
26. Iijima, S., "Helical Microtubules of Graphite Carbon," Nature, 354, 56-58, 1991.
27. Iijima, S., and T. Ichihashi, "Single-shell Carbon Nanotubes of 1-nm Diameter," Nature, 363, 603-605, 1993.
28. Bethune, D.S., C.H. Kiang, M.S. DeVries, G. Gorman, R. Savoy, J. Vazquez, and Beyers, R., "Cobalt Catalyzed Growth of Carbon Nanotubes with Single Atomic Layer Walls," Nature, 363, 605-607, 1993.
29. Nicodemus, F.E., J.C. Richmond, J.J. Hsia, I.W. Ginsburg, and T. Limperis, "Geometrical Considerations and Nomenclature for Reflectance," National Bureau of Standards, NBS Monograph 160, 1977.
30. Taylor, B.E. and C.E. Kuyatt, "Guidelines for Evaluating and Expressing the Uncertainty of NIST Measurement Results," NIST Technical Note 1297, U.S. Department of Commerce, National Institute of Standards and Technology, 1977.
31. Schiff, T.F., M.W. Knighton, D.J. Wilson, F.M. Cady, J.C. Stover, and J.J. Butler, "A Design Review of a High Accuracy UV to Near Infrared Scatterometer," Proc. SPIE, 1995, 121-130, 1993.
32. Getty, S.A., R.A. Bis, S. Snyder, E. Gehrels, K. Ramirez, T.T. King, P. A. Roman, and P.R. Mahaffy, "Effect of Nitrogen Gas on the Lifetime of Carbon Nanotube Field Emitters for Electron-impact Mass Spectrometry," Proc. SPIE, 6959, 695907-1 to 695907-10, 2008.